Reactions of Mn with H_2O and MnO with H_2. Matrix-Isolation FTIR and Quantum Chemical Studies

Mingfei Zhou,*,†,‡ Luning Zhang,†,‡ Limin Shao,†,‡ Wenning Wang,† Kangnian Fan,† and Qizong Qin†,‡

Department of Chemistry, Fudan University, Shanghai 200433, People's Republic of China, and Laser Chemistry Institute, Fudan University, Shanghai 200433, People's Republic of China

Received: November 28, 2000; In Final Form: February 14, 2001

The reactions of Mn atoms with water and MnO with H_2 have been studied using matrix-isolation FTIR and DFT theoretical calculations. In solid argon, Mn atom reacted with H_2O molecule to form the $MnOH_2$ complex spontaneously. Photolysis destroyed the $MnOH_2$ complex and produced the inserted HMnOH molecule. In addition, HMnOMnH, $Mn(OH)_2$, HMnOMnOH, and posssibly HMnOMnOMnH molecules were also produced on photolysis. Reaction of MnO with H_2 gave the $(H_2)MnO$ complex without activation energy. Photolysis of the $(H_2)MnO$ produced the inserted HMnOH molecule as well. The aforementioned species were identified via isotopic substitutions as well as density functional theoretical frequency calculations. Potential energy surface for the $Mn + H_2O \leftrightarrow MnO + H_2$ reaction was also given. Our calculation results showed that all these reaction intermediates and products are high spin molecules. The $MnOH_2$, HMnOH and $(H_2)MnO$ molecules have ground states with $S = {}^5/_2$, the HMnOMnH, and HMnOMnOH molecules have ground states with $S = {}^{10}/_2$, and the HMnOMnOMnH molecule has ground state with $S = {}^{15}/_2$.

Introduction

The interaction of transition metal centers with water molecules is of interest in a wide variety of areas, including catalytic synthesis, surface chemistry. and biochemical systems. Previous experimental and theoretical studies have provided a wealth of insight concerning the reactivity of transition metal atoms and ions with water molecules.[1−14] The reaction of manganese with water is of particular interest in biochemical systems. It is generally thought that the reaction center of photosystem II binds the Mn cluster that catalyzes the oxidation of water. Photosystem II is a key enzyme located in the thylakoid membranes in green plants, algae and cyanobacteria.[15] It catalyzes the light driven electron transfer from water to the membrane bound electron carrier plastoquinone. In the process, water molecules are oxidized to molecular oxygen. Although interaction of water with manganese cluster complexes has gained intensive attention,[16] the reaction of Mn atom with water molecule has attracted much less attention. Using matrix-isolation infrared absorption method, Kauffman et al. showed that thermal manganese atom formed adduct with water, which was rearranged to the inserted HMnOH molecule on photolysis.[2]

The H−H activation by metal monoxide provides a simple system to study in detail, and serves as a model for other reactions of metal oxide with organic substrates.[17] Previous gas-phase studies have demonstrated that monoxide cations of the late row transition metals Mn, Fe, Co, and Ni are more reactive than their bare metal cation analogues.[18−24] Recent studies showed that these MO^+ ions are able to oxidize H_2 and small organic molecules at thermal energy; apparently, the oxo ligand increased the reactivity of the bare metal cations. To our knowledge, there is no report on the reactions of neutral transition metal monoxides with H_2 molecule.

Recently, we have performed matrix-isolation FTIR and theoretical studies of the reactions of laser-ablated early transition metal atoms (Sc, Ti, and V group) with water molecules in solid argon.[25−27] Different reaction paths leading to the H_2-MO and $MO + H_2$ were observed. In particular, the combination of experimental and theoretical approaches has been extremely beneficial in understanding and interpreting the reaction mechanisms and periodic trends for the early transition metal−water reactions. Here we report a study of reactions of laser-ablated Mn atom with water and manganese monoxide with hydrogen in solid argon. Although this study seems parallel to that of early transition metal atoms with water, we will show that it is distinctly different because of the intrinsic differences between Mn and early transition metals.

Experimental and Theoretical Methods. The experimental setup for pulsed laser ablation and matrix infrared spectroscopic investigation has been described previously.[25−28] The 1064 nm Nd:YAG laser fundamental (Spectra Physics, DCR 150, 20 Hz repetition rate, and 8 ns pulse width) was focused onto the rotating manganese metal or dioxide targets through a hole in a CsI window, and the ablated species were co-deposited with reagent gas in excess argon onto a 11K CsI window, which was mounted on a cold tip of a closed-cycle helium refrigerator (Air Products, model CSW202) for 1 h at a rate of 2−4 mmol/h. Typically, 5−20 mJ/pulse laser power was used. H_2O, $H_2{}^{18}O$-(96%^{18}O) and D_2O were subjected to several freeze−pump−thaw cycles before use. Infrared spectra were recorded on a Bruker IFS113V spectrometer at 0.5 cm^{-1} resolution using a DTGS detector. Matrix samples were annealed at different temperatures, and selected samples were subjected to broadband photolysis using a high-pressure mercury lamp.

Quantum chemical calculations were performed using the Gaussian 98 program.[29] The three parameter hybrid functional according to Becke with additional correlation corrections due to Lee, Yang, and Parr were utilized (B3LYP).[30,31] Recent

† Department of Chemistry.
‡ Laser Chemistry Institute.

10.1021/jp0043118 CCC: $20.00
Published on Web 05/30/2001

TABLE 1: Infrared Absorptions (cm^{-1}) from Co-Deposition of Laser-Ablated Mn Atoms with H_2O Molecules in Excess Argon

H_2O	D_2O	$H_2{}^{18}O$	$H_2O + HDO + D_2O$	$H_2{}^{16}O + H_2{}^{18}O$	assignment (mode)[a]
1663.4	1197.8	1163.4	1663.4,1197.8		HMnOH (Mn−H)
1644.4	1182.4	1644.6	1644.4,1182.4		HMnOMnOH (Mn−H)
1638.5	1175.3	1638.6	1641.8,1638.5, 1179.5, 1175.3		HMnOMnH (asy-MnH)
1627.7		1627.8			(HMnOMnOMnH) (asy-MnH)
1576.6	1166.0	1570.0	1576.6, 1388.5, 1166.0	1576.6,1570.0	$MnOH_2$ (H_2O bending)
884.8	884.6	841.9		884.8,841.9	HMnOMnOH (asy-MnOMn)
875.1	875.2	835.0			(HMnOMnOMnH) (asy-OMnO)
870.5	870.3	827.6		870.5,827.6	HMnOMnH (asy-MnOMn)
833.3	833.3	796.7		833.3,796.7	MnO (Mn−O)
709.0	693.6	687.3	709.0,701.9, 693.6	709.0,699.3, 687.3	$Mn(OH)_2$ (asy-Mn−OH)
648.6	628.7	624.3		648.6,624.3	HMnOH (Mn−OH)

[a] sym = symmetric; asy = asymmetric.

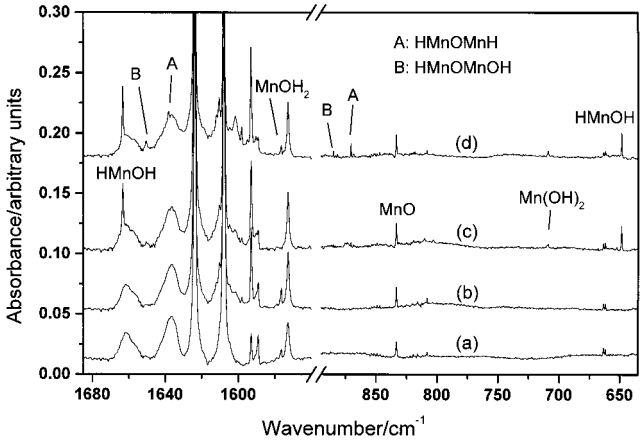

Figure 1. Infrared spectra in the 1670−1560 and 895−635 cm^{-1} regions from co-deposition of laser-ablated Mn with 0.2% H_2O in argon. (a) 1 h sample deposition at 11 K, (b) after 25 K annealing, (c) after 20 min photolysis, and (d) after 30 K annealing.

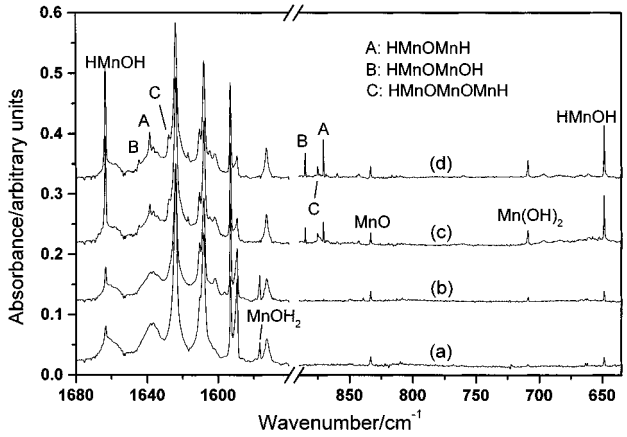

Figure 2. Infrared spectra in the 1670−1560 and 895−635 cm^{-1} regions from co-deposition of laser-ablated Mn with 0.4% H_2O in argon. (a) 1 h sample deposition at 11 K, (b) after 25 K annealing, (c) after 20 min photolysis, and (d) after 30 K annealing.

calculations have shown that this hybrid functional can provide very reliable predictions of the state energies, structures and vibrational frequencies of transition metal containing compounds.[32−36] The 6-311++G(d,p) basis sets were used for H and O atoms, and the all electron basis sets of Wachters-Hay as modified by Gaussian were used for Mn atom.[37,38] The geometries were fully optimized, and harmonic vibrational frequencies calculated with analytic second derivatives, and zero point vibrational energies (ZPVE) were derived. Transition state optimizations were done with the synchronous transit-guided quasi-Newton(STQN) method at the B3LYP/6-311++G(d,p) level,[39] followed by the vibrational frequency calculations showing that the obtained structures to be true saddle points. In addition, the IRC calculations were performed to verify the transition states connecting the reactant and product on the potential energy surface.

Results and Discussion

Experimental Results. *Mn + H_2O/Ar*. Experiments were performed with different laser power and water concentrations; the observed product absorptions and assignments are listed in Table 1. Representative spectra in the Mn−H stretching and Mn−O stretching vibrational frequency regions using lower laser power and 0.2% H_2O in argon are shown in Figure 1. The major new product absorptions observed after sample deposition were 1663.4, 1576.6, and 648.6 cm^{-1}. Annealing to 25 K increased the 1576.6 cm^{-1} absorption with no obvious change on 1663.4 and 648.6 cm^{-1} absorptions. Photolysis destroyed the 1576.6 cm^{-1} absorption but greatly enhanced the 1663.4 and 648.6 cm^{-1} absorptions. In addition, new absorptions at 1644.4, 1638.5, 884.8, 870.5, and 709.0 cm^{-1} were also produced on photolysis. Figure 2 shows the spectra with 0.4% H_2O in argon using slightly higher laser power. The new product absorptions in Figure 1 were also observed here but with higher intensities. In contrast to Figure 1, weak new absorptions at 1627.7 and 875.1 cm^{-1} were produced on photolysis.

Isotopic substitution was employed for band identification, and the results are also listed in Table 1. Figures 3−5 show the mixed $H_2O + HDO + D_2O$ and $H_2{}^{16}O + H_2{}^{18}O$ spectra in selected regions, and the isotopic splittings will be discussed below.

MnO_2+H_2/Ar. First, an experiment was performed with a MnO_2 target and pure argon gas, and the spectrum after deposition is shown in Figure 6a. The major product absorptions are 833.3, 947.8, and 816.3 cm^{-1} due to MnO and MnO_2; weak absorptions of MnO_2^- (858.3 cm^{-1}) and MnOMn (808.3 cm^{-1}) were also observed.[40] MnO + H_2 reactions were performed with laser ablation of MnO_2 in 1.0% H_2 in argon, the product absorptions are listed in Table 2, and infrared spectra in the Mn−O stretching vibrational frequency region are shown in Figure 6b−d. The MnO, MnO_2, MnO_2^-, and MnOMn absorp-

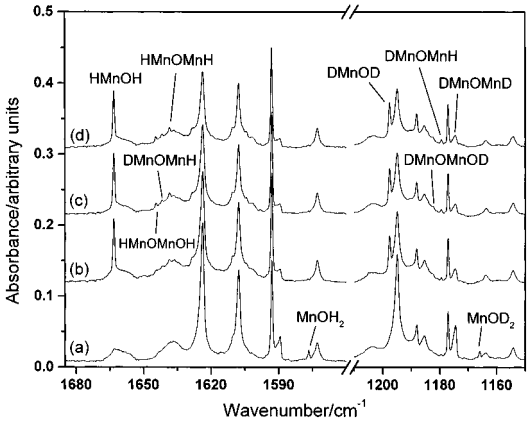

Figure 3. Infrared spectra in the 1670−1560 and 1210−1160 cm^{-1} regions from co-deposition of laser-ablated Mn with 0.6%(H_2O + HDO + D_2O) in argon. (a) 1 h sample deposition at 11 K, (b) after 20 min photolysis, (c) after 28 K annealing, and (d) after 32 K annealing.

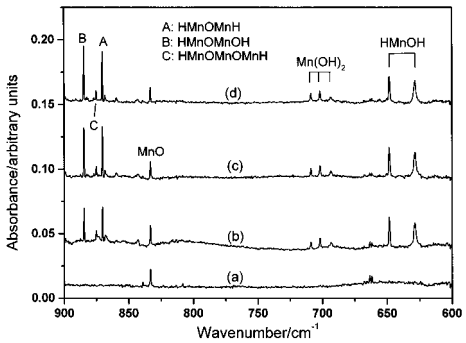

Figure 4. Infrared spectra in the 900−610 cm^{-1} region from co-deposition of laser-ablated Mn with 0.6%(H_2O + HDO + D_2O) in argon. (a) 1 h sample deposition at 11 K, (b) after 20 min photolysis, (c) after 28 K annealing, and (d) after 32 K annealing.

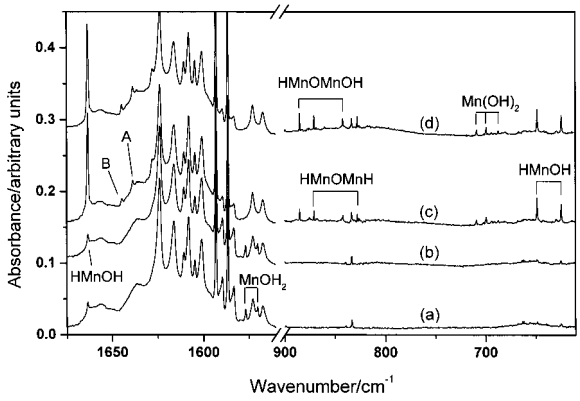

Figure 5. Infrared spectra in the 1670−1560 and 900−610 cm^{-1} regions from co-deposition of laser-ablated Mn with 0.6%($H_2{}^{16}O$ + $H_2{}^{18}O$) in argon. (a) 1 h sample deposition at 11 K, (b) after 25K annealing, (c) after 20 min photolysis, and (d) after 28 K annealing.

tions were observed as in Figure 6a, and new absorption at 849.7 cm^{-1} was observed after sample deposition, which slightly increased on 20K annealing. Photolysis destroyed the 849.7 cm^{-1} absorption and produced two new absorptions at 1663.4 and 648.6 cm^{-1}.

Calculation Results. DFT calculations were performed on the potential products observed in present experiments. Calculations were performed on three isomers of MnH_2O, namely, the $MnOH_2$ complex, the inserted HMnOH molecule, and the (H_2)-MnO complex. The optimized geometric parameters and relative stability are shown in Figure 7, and the vibrational frequencies

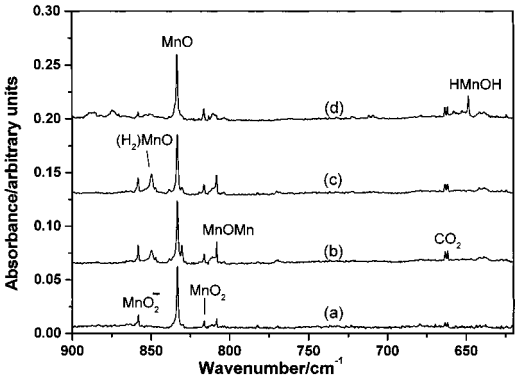

Figure 6. Infrared spectra in the 900−620 cm^{-1} regions from co-deposition of laser-ablated MnO_2 with (a) pure argon, 1 h sample deposition at 11 K, (b) 1.0% H_2 in argon, 1 h sample deposition at 11 K, (c) 25 K annealing of sample (b), and (d) after 20 min photolysis of sample (c).

TABLE 2: Infrared Absorptions (cm^{-1}) from Co-Deposition of Laser-Ablated MnO_2 with H_2 Molecules in Excess Argon

	assignment (mode)[a]
1663.4	HMnOH (Mn−H)
947.8	MnO_2 (asy-MnO_2)
858.3	MnO_2^- (asy-MnO_2)
849.7	(H_2)MnO (Mn−O)
833.3	MnO (Mn−O)
816.3	MnO_2 (sym-MnO_2)
808.3	MnOMn (asy-MnOMn)
648.6	HMnOH (Mn−OH)

[a] sym = symmetric; asy = asymmetric.

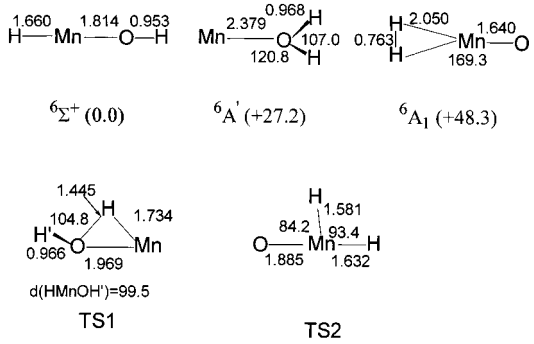

Figure 7. B3LYP/6-311++G(d,p) calculated geometric parameters (bond length in angstroms, bond angle in degrees) and relative stability (in kcal/mol) of the MnH_2O isomers and the transition states in the Mn + H_2O reaction path.

TABLE 3: Calculated Vibrational Frequencies (cm^{-1}) and Intensities (km/mol) for the $MnOH_2$, HMnOH, (H_2)MnO, and the Transition States (TS1, TS2) on the Mn + H_2O Reaction Path

$MnOH_2$	HMnOH	(H_2)MnO	TS1	TS2
3824(58, a″)	4000(142, σ)	4089(9, a_1)	3803(36)	1773(206)
3705(99, a′)	1729(204, σ)	905(209, a_1)	1379(13)	1721(2)
1597(83, a′)	691(143, σ)	847(29, b_2)	673(104)	619(83)
317(0.4, a″)	290(286, π)	462(1, a_1)	478(125)	261(130)
181(182, a′)	44(318, π)	213(0.2, b_1)	336(152)	245(125)
141(1, a′)		198(0, b_2)	1142i(961)	316i(11)

and intensities are listed in Table 3. At the B3LYP/6-311++G-(d,p) level of theory, all three MnH_2O isomers were calculated to have sextet ground states. The $^6\Sigma^+$ HMnOH is the global minimum, the $^6A'$ $MnOH_2$ is 27.2 kcal/mol higher and the $^6A_1$ (H_2)MnO is 48.3 kcal/mol higher than the global minimum.

Similar calculations were done for $Mn(OH)_2$, HMnOMnH, HMnOMnOH and HMnOMnOMnH molecules. The optimized

TABLE 4: Calculated Vibrational Frequencies (cm^{-1}) and Intensities (km/mol) for the Structures Described in Figure 8

molecule	frequency(intensity, mode)
$Mn(OH)_2$	3945.4(13, a), 3944.9(183, b), 734(237, b), 608(6, a), 411(82, a),
(^6A)	381(242, a), 133(14, b), 127(2, b), 110(111,a)
HMnOMnH	1709(0, σ_g), 1700(575, σ_μ), 850(794, σ_μ), 332(0, σ_g), 265(0, π_g),
($^{11}\Sigma_\mu^+$)	261(652, π_μ), 91(2, π_μ)
HMnOMnOH	3947(103,a′), 1701(275,a′), 865(837,a′), 673(83,a′), 400(171,a′),
($^{11}A'$)	311(5, a′), 260(178, a"), 253(171, a′), 144(2, a"), 138(15, a′),
	68(21, a″), 59(2, a′)
HMnOMnOMnH	1698(0,σ_g), 1696(590, σ_μ), 869(0, σ_g), 849(1910, σ_μ), 405(7,σ_μ),
($^{16}\Sigma_\mu^+$)	260(670, π_μ), 259(0, π_g), 229(0, σ_g), 142(40, π_μ), 85(0, π_g),29(2, π_μ)

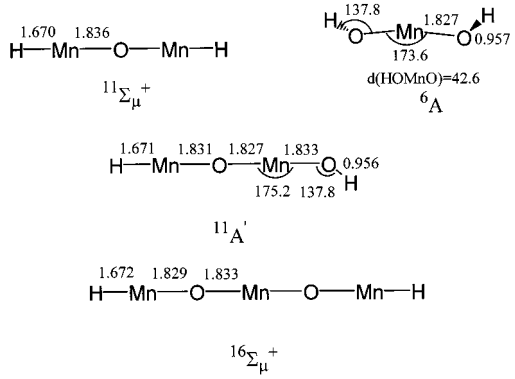

Figure 8. B3LYP/6-311++G(d,p) calculated geometric parameters (bond length in angstroms, bond angle in degrees) of the HMnOMnH, $Mn(OH)_2$, HMnOMnOH, and HMnOMnOMnH molecules.

TABLE 5: The Scaling Factors and the Observed and Calculated Isotopic Vibrational Frequency Ratios of the Major Reaction Products

			H/D		$^{16}O/^{18}O$	
molecule	mode[a]	scaling factor	obsd	calcd	obsd	calcd
$MnOH_2$	OH_2 bend	0.988	1.3521	1.3635	1.0042	1.0044
HMnOH	Mn−H	0.962	1.3887	1.4140	1.0000	1.0000
	Mn−OH	0.939	1.0317	1.0258	1.0389	1.0430
HMnOMnH	asy-Mn−H	0.964	1.3947	1.4023	1.0000	1.0000
	asy-MnOMn	1.025	1.0002	1.0002	1.0518	1.0525
$Mn(OH)_2$	asy-Mn−OH	0.966	1.0222	1.0214	1.0316	1.0324
HMnOMnOH	Mn−H	0.967	1.3907	1.4016	1.0000	1.0000
	asy-MnOMn	1.023	1.0002	1.0002	1.0510	1.0514

[a] sym = symmetric; asy = asymmetric, bend = bending.

geometries are shown in Figure 8, and the vibrational frequencies and intensities are summarized in Table 4.

Detailed structural parameters, absolute energies, vibrational frequencies for different spin state molecules and atomic spin density on Mn centers for the ground-state molecules are given as Supporting Information.

Product Identification. *$MnOH_2$.* The 1576.6 cm^{-1} band in the Mn + H_2O/Ar experiments is assigned to the $MnOH_2$ complex, in agreement with previous assignment.[2] This band produced a triplet with H_2O + HDO+D_2O sample and a doublet with $H_2{}^{16}O$ + $H_2{}^{18}O$ sample as required for a product with one H_2O unit. The isotopic H/D ratio of 1.3521 and $^{16}O/^{18}O$ ratio of 1.0042 indicate a H_2O bending vibration. DFT calculations on $MnOH_2$ predicted that the molecule have a sextet ground state ($^6A'$ under C_s symmetry) that correlated to the Mn ^6S ground state. The calculated H_2O bending frequency, 1597 cm^{-1}, is in quite good agreement with the experimental value. As shown in Table 5, the calculated isotopic frequency ratios agree well with the experimental values.

$(H_2)MnO$. The 849.7 cm^{-1} band in the laser ablation of MnO_2 and H_2 experiments increased on annealing, but was destroyed on photolysis when the HMnOH absorptions were produced. This band was not observed in the experiment of laser ablation of MnO_2 in pure argon, suggesting a reaction product of laser-ablated species with H_2. Although it is hard to make a definitive assignment without isotopic substitution, in light of the above behavior and the only 16.4 cm^{-1} blue shift from the MnO, we suggest assignment of this band to the $(H_2)MnO$ complex by comparison with the $(O_2)MnO$ in the Mn + O_2 system.[40] The assignment gained further support from DFT calculations. The $(H_2)MnO$ molecule was predicted to have a $^6A_1$ ground state with C_{2v} symmetry that correlated to the ground state $^6\Sigma^+$ MnO.[41] Although the $^6A_1$ state $(H_2)MnO$ is higher in energy than the $MnOH_2$ and HMnOH isomers, it is a true minimum on the sextet potential energy surface. The Mn−O and H−H stretching vibrations were predicted at 905 and 4089 cm^{-1} with 209:9 relative intensities. The H−H stretching vibration is too weak to be observed in present experiments.

HMnOH. In both the Mn + H_2O and MnO_2 + H_2 experiments, sharp bands at 1663.4 and 648.6 cm^{-1} greatly enhanced in concert on photolysis, suggesting different vibrational modes of the same molecule. The increase upon photodestruction of $MnOH_2$ (Mn + H_2O experiments) or $(H_2)MnO$ (MnO_2 + H_2 experiments) implies that this molecule is generated from $MnOH_2$ or $(H_2)MnO$ The 1663.4 cm^{-1} band showed no oxygen-18 shift, but shifted to 1197.8 cm^{-1} with D_2O sample. The isotopic H/D ratio of 1.3887 indicates that this band is due to a Mn−H stretching vibration. The 648.6 cm^{-1} band shifted to 628.7 cm^{-1} with D_2O and to 624.3 cm^{-1} with $H_2{}^{18}O$, which define a H/D ratio of 1.0317 and a $^{16}O/^{18}O$ ratio of 1.0389. Isotopic substitution showed that this band is Mn−OH in vibrational character. The mixed H_2O + HDO+D_2O and $H_2{}^{16}O$ + $H_2{}^{18}O$ isotopic spectra revealed that only one H atom is involved in the upper mode and one OH is involved in the low mode. These two absorptions are assigned to the Mn−H and Mn−OH stretching vibrations of the HMnOH molecule. The assignment is in good agreement with previous thermal atom experiments.[2] The HMnOH was predicted to have a $^6\Sigma^+$ ground state, with configuration of (core)$\sigma^2\pi^4\delta^2\sigma^2\pi^2\sigma^1$, where the five unpaired electrons are mainly of Mn 3d-based character. The geometry of HMnOH ground state is predicted to be linear with H−Mn, Mn−O and O−H bond lengths of 1.660, 1.814 and 0.953 Å, respectively. The vibrational frequencies of Mn−H and Mn−OH stretching modes were calculated to be 1729 and 691 cm^{-1}, which require scaling factors of 0.962 and 0.939 to fit the experimental values.

HMnOMnH. The 870.5 cm^{-1} band in the Mn + H_2O experiments was produced only on photolysis. This band exhibited $H_2{}^{18}O$ counterpart at 827.6 cm^{-1}. In the mixed $H_2{}^{16}O$ + $H_2{}^{18}O$ experiments, only pure isotopic counterparts were observed, indicating that only one O atom is involved in this mode. The $^{16}O/^{18}O$ ratio of 1.0518 is quite higher than the diatomic MnO ratio of 1.0460, suggesting an antisymmetric MnOMn stretching mode. This band showed 0.2 cm^{-1} deuterium isotopic shift, which indicates that this mode is slightly coupled by H atoms. The 870.5 cm^{-1} band is associated with a

1638.5 cm^{-1} band. This band underwent a large deuterium shift, but no apparent oxygen shift. In the mixed $H_2O + HDO + D_2O$ experiment, two intermediates at 1641.8 and 1179.5 cm^{-1} were produced, the mixed isotopic spectra are typical for linear H−M-H type molecules. Accordingly, the 870.5 and 1638.5 cm^{-1} bands are assigned to the antisymmetric MnOMn and H−MnOMn−H stretching vibrations of the HMnOMnH molecule. The 1641.8 and 1179.5 cm^{-1} bands in the mixed experiment are due to H−Mn and D-Mn stretching vibrations of the HMnOMnD molecule.

As ground-state Mn has $3d^5 4s^2$ valence electron configuration, one can draw a convenient Lewis structure that satisfies the valence of H and O:

$$H-\overset{\cdot\cdot\cdot\cdot\cdot}{Mn}-O-\overset{\cdot\cdot\cdot\cdot\cdot}{Mn}-H$$

In this structure, the 4s electrons of Mn are used to form covalent bonds with H and O atoms, and the Mn 3d electrons remain unpaired. This suggests that HMnOMnH should have a ground state with $S = {}^{10}/_{2}$. Consistent with this simple formulation, our DFT calculations predicted that the molecule has a $^{11}\Sigma_\mu^+$ ground state with linear geometry, and the 10 unpaired metal-based electrons occupying the nonbonding or antibonding d_π, d_δ, and d_σ orbitals. The antisymmetric MnOMn and H−MnOMn−H stretching vibrations of the ground-state molecule were calculated at 850 and 1700 cm^{-1}, with 794:575 relative intensities. As listed in Table 5, the calculated isotopic frequency ratios are in excellent agreement with the observed values.

$Mn(OH)_2$. The 709.0 cm^{-1} band appeared on photolysis, and is favored by slightly higher water concentrations. It shifted to 693.6 cm^{-1} with D_2O and to 687.3 cm^{-1} with $H_2{}^{18}O$, giving a H/D ratio of 1.0222 and a $^{16}O/^{18}O$ ratio of 1.0316. The mixed $H_2O + HDO + D_2O$ and $H_2{}^{16}O + H_2{}^{18}O$ isotopic spectra revealed triplet isotopic structure and clearly indicate that two equivalent O and H atoms are involved in this mode. The isotopic shifts and mixed isotopic splittings suggest an assignment to the $Mn(OH)_2$ species. The above assignment is confirmed by DFT calculations. As shown in Figure 8, the $Mn(OH)_2$ is predicted to have a ^6A ground state, with the five unpaired electrons mainly located on the Mn center which are mainly Mn 3d in character. The ground state is predicted to be nonlinear ($\angle OMnO = 173.6°$ and $\angle MnOH = 137.8°$); the two H atoms are slightly out of OMnO plane. The linear geometry is predicted to be slightly higher in energy and has one imaginary frequency. The antisymmetric and symmetric Mn−OH stretching vibrations in the ground-state molecule were calculated at 734 and 608 cm^{-1} with 237:6 relative intensities. The symmetric stretching vibrational frequency is lower than that of the antisymmetric vibration and is not observed in our experiments due to weakness. The calculated isotopic frequency ratios of the observed antisymmetric stretching mode (H/D: 1.0214, $^{16}O/^{18}O$:1.0324) are in excellent agreement with the experimental values.

HMnOMnOH. The 884.8 and 1644.4 cm^{-1} bands were produced upon photolysis, these two bands showed exactly the same annealing behavior and maintained the same relative intensities in different experiments, suggesting different vibrational modes of the same molecule. These bands were favored with slightly higher water concentrations and higher laser power. The 1644.4 cm^{-1} band shifted to 1182.4 cm^{-1} with D_2O, but no apparent shift with $H_2{}^{18}O$, and is assigned to a Mn−H stretching mode. In the mixed $H_2O + HDO + D_2O$ isotopic spectra, no obvious intermediate absorption was observed, indicating that only one H atom is involved in this vibrational mode. The 884.8 cm^{-1} band underwent a very small deuterium shift (0.2 cm^{-1}), but shifted to 841.9 cm^{-1} with $H_2{}^{18}O$, and gave an isotopic $^{16}O/^{18}O$ ratio of 1.0510. This ratio suggests an antisymmetric MnOMn stretching mode analogous to the 870.5 cm^{-1} band. In light of the above, assignment to HMnOMnOH is suggested. The bonding of HMnOMnOH molecule is quite similar to the HMnOMnH molecule. DFT calculations predicted that the linear HMnOMnOH molecule has a $^{11}\Sigma^+$ ground state, but has an imaginary frequency. Therefore, we search for minimum energy structure in bent geometry, as shown in Figure 8, the bent structure with an MnOH angle of 137.8° is about 0.3 kcal/mol lower in energy than the linear structure and has no imaginary frequency. As the potential surface for bending of the MnOH unit is very flat, it is difficult to determine whether this molecule is linear or not. The Mn−H and antisymmetric MnOMn stretching vibrations for the $^{11}A'$ HMnOMnOH molecule were predicted at 1701 and 865 cm^{-1}. The MnOH stretching vibration was calculated at 673 cm^{-1} with one-tenth intensity of the antisymmetric MnOMn stretching mode, and is under noise level. The calculated isotopic shifts are also in very good agreement with experimental values (see Table 5).

(HMnOMnOMnH). The 1627.7 and 875.1 cm^{-1} bands were presented only at higher laser power and medium water concentration experiments. These two bands appeared together on photolysis. The mixed isotopic structures could not be resolved due to isotopic dilution. These two bands are tentatively assigned to the antisymmetric H−MnOMnOMn−H and O−Mn−O stretching vibrations of the HMnOMnOMnH molecule. Our DFT calculations predicted the HMnOMnOMnH to have a $^{16}\Sigma_\mu^+$ ground state with linear geometry. The bonding of this molecule is quite similar to the HMnOMnH and HMnOMnOH molecules. The 4s electrons of Mn atoms are used to form covalent bonds to satisfy the valence of H and O atoms, and the unpaired electrons are located on the three Mn centers. The two vibrational modes were calculated at 1695 and 849 cm^{-1}.

Reaction Mechanism. Laser-ablated Mn atoms co-deposited with water to form the $MnOH_2$ complex at low temperature, and the $MnOH_2$ absorption increased on annealing, suggesting that reaction 1 requires no activation energy. The $MnOH_2$ absorption was destroyed on photolysis. The increase of HMnOH absorptions upon photodestruction of the $MnOH_2$ implies that the HMnOH molecule is generated from $MnOH_2$ via reaction 2, which was predicted to be exothermic by about 27.2 kcal/mol.

$$Mn(^6S) + H_2O(^1A_1) \rightarrow MnOH_2(^6A') \qquad \Delta E = -34.6 \text{ kcal/mol} \quad (1)$$

$$MnOH_2(^6A') \rightarrow HMnOH(^6\Sigma^+) \qquad \Delta E = -27.2 \text{ kcal/mol} \quad (2)$$

The reactions of early transition metal atoms with water molecules have been recently studied in this laboratory.[25−27] For Sc, Ti, and V, the inserted HMOH molecules were produced spontaneously, and broadband photolysis produced the covalently bonded H_2MO molecules as well as the MO monoxides. In present Mn + H_2O reaction, no H_2MnO molecule was produced. Although the MnO molecule absorption was observed, the MnO absorption did not enhance on photolysis. In the $H_2{}^{18}O$ experiments, no $Mn^{18}O$ absorption was observed, indicating that the observed MnO molecule was not the product of water reaction.

Although dehydrogenation process is not observed for Mn + H_2O reaction, co-deposition of laser-ablated MnO with H_2 formed the $(H_2)MnO$ spontaneously. On photolysis, the HMnOH

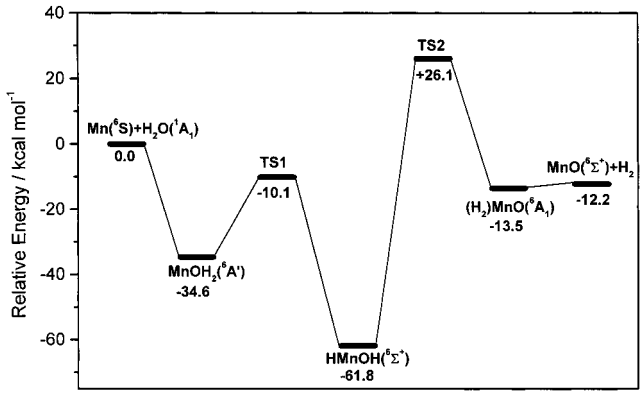

Figure 9. Potential energy surface following the Mn + H_2O → MnO + H_2 reaction path. Energies given are in kcal/mol and are relative to the separated ground-state reactants: Mn(^{6}S) + H_2O($^1A_1$).

absorptions were produced at the expense of the $(H_2)MnO$. Certainly the growth of the $(H_2)MnO$ molecule on annealing suggests a spontaneous reaction 3, although this reaction was predicted to be exothermic by only about 1.3 kcal/mol. The isomerization reaction 4 was predicted to be exothermic by about 48.3 kcal/mol, this reaction requires activation energy.

$$MnO(^6\Sigma^+) + H_2(^1\Sigma_g+) \rightarrow (H_2)MnO(^6A_1) \qquad \Delta E = -1.3 \text{ kcal/mol} \quad (3)$$

$$(H_2)MnO(^6A_1) \rightarrow HMnOH(^6\Sigma^+) \qquad \Delta E = -48.3 \text{ kcal/mol} \quad (4)$$

Figure 9 shows the potential energy surface starting from the separated Mn + H_2O and leading to the MnO + H_2 for the sextet state at the B3LYP/6-311++G(d,p) level of theory. The first step of Mn and water interaction is the formation of the $MnOH_2$ complex. The $MnOH_2$ complex has a $^6A'$ ground state with nonplanar geometry. Becausethe separation between the $3d^54s^2$ ground state and the $3d^64s^1$ excited state of Mn atom is very large (49 kcal/mol),[42] the $4s-3d_\sigma$ hybridization to reduce the σ repulsion is not possible. The only mechanism for Mn to reduce the repulsion is by 4sp polarization away from water. Apparently, this is not very efficient, thus that water tilts to further reduce the Mn−water lone pair repulsion.

From $MnOH_2$ complex, one hydrogen atom is passed from oxygen to the Mn, leading to the HMnOH intermediate through TS1. This process involves the breaking of one H−O bond, and the formation of a Mn−H bond and a Mn−O bond by overcoming an energy barrier of 24.5 kcal/mol. The TS1 transition state lies 10.1 kcal/mol below the energy of the ground-state reactants. Geometric parameters of this transition state can be found in Figure 7. This transition state has nonplanar geometry, and the one imaginary frequency reflects the H−O bond breaking and the Mn−H bond formation. The IRC calculation also indicates that TS1 connects the $MnOH_2$ complex and the HMnOH molecule on the potential energy surface.

From linear HMnOH, the second hydrogen transfers from oxygen to form the $(H_2)MnO$ through transition state 2. This process involves the breaking of the Mn−H and O−H bonds, and the formation of a H−H bond and a Mn−O π bond. The geometric parameters of transition state 2 are also given in Figure 7. This transition state shows quite long Mn−O bond distance (1.885 Å), suggesting a Mn−O single bond. The two Mn−H bond distances 1.581 and 1.632 Å indicate that both Mn−H are mainly covalent bonds. From the $(H_2)MnO$, the loss of H_2 proceeds without transition state to the MnO + H_2. This $(H_2)MnO$ intermediate has planar C_{2v} symmetry; the Mn−H distances were predicted to be quite long (2.050 Å). This minimum has no Mn−H covalent bonding character, and should be considered as a complex. The Mn−O and H−H bond lengths in this complex are about 0.003 and 0.019 Å longer than that of diatomic MnO and H_2.

The transition state 2 lies 26.1 kcal/mol higher in energy than the separated Mn + H_2O reactants. Reaction from HMnOH to $(H_2)MnO$ is predicted to be endothermic by about 48.3 kcal/mol; there is about 87.9 kcal/mol energy barrier. Apparently, this reaction is hardly to be observed in present experimental conditions. In contrast, the reverse reaction: $(H_2)MnO$ → HMnOH is exothermic, and the energy barrier is only about 39.6 kcal/mol. This reaction is observed upon photolysis in the MnO + H_2 reaction system.

In the Mn + H_2O reaction system, the HMnOMnH absorptions appeared on photolysis, suggesting that Mn atoms can further react with HMnOH via reaction 5. This reaction was predicted to be exothermic by about 65.3 kcal/mol.

$$HMnOH(^6\Sigma^+) + Mn(^6S) \rightarrow HMnOMnH(^{11}\Sigma_\mu^+) \qquad \Delta E = -65.3 \text{ kcal/mol} \quad (5)$$

The $Mn(OH)_2$ absorption was also produced on photolysis, this molecule is most probably formed by reaction of Mn atom and water dimer via reaction 6. This reaction was calculated to be exothermic by about 82 kcal/mol.

$$Mn(^6S) + (H_2O)_2 \rightarrow Mn(OH)_2(^6A) + H_2(^1\Sigma_g^+) \qquad \Delta E = -82.0 \text{ kcal/mol} \quad (6)$$

In higher laser power experiments, photolysis also produced the HMnOMnOH and possibly the HMnOMnOMnH absorptions, suggesting that Mn atoms can further react with $Mn(OH)_2$ molecules via reactions 7 and 8, which were predicted to be quite exothermic:

$$Mn(OH)_2(^6A) + Mn(^6S) \rightarrow HMnOMnOH(^{11}A') \qquad \Delta E = -66.0 \text{ kcal/mol} \quad (7)$$

$$HMnOMnOH(^{11}A') + Mn(^6S) \rightarrow HMnOMnOMnH(^{16}\Sigma_\mu^+) \qquad \Delta E = -65.8 \text{ kcal/mol} \quad (8)$$

In previous thermal Mn atom and water reaction studies, only the HMnOH and HMnOMnH molecules were produced on photolysis with 300−340 nm using a 100W medium-pressure mercury lamp.[2] To have a better understanding of the photolysis behavior, experiments were performed with different wavelength range high-pressure mercury lamp photolysis. The HMnOH molecules were produced after 20 min photolysis with a 400 nm long-wavelength pass filter. The $Mn(OH)_2$, HMnOMnH and HMnOMnOH absorptions were produced on photolysis with λ > 290 nm photolysis, and the HMnOMnOMnH absorptions were mainly produced on full arc photolysis.

The results on Mn + H_2O system are different from the early transition metal Sc, Ti and V +H_2O systems.[25−27] As Sc has only three valence electrons, the only exothermic reaction path observed is the formation of ScO + H_2. For Ti and V systems, two exothermic reaction paths have been observed: the formation of H_2MO and MO + H_2. (M = Ti, V). Although the Mn + H_2O → MnO + H_2 reaction was predicted to be slightly exothermic (−12.2 kcal/mol), the MnO was not formed, as proof of the existence of the high energy barrier for the transformation of HMnOH to $(H_2)MnO$. The H_2MnO was not formed either. Our calculations showed that the ground state of H_2MnO is a quartet state, and is higher in energy than the sextet $(H_2)MnO$.

SCHEME 1

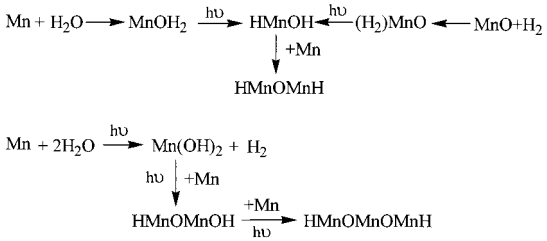

The formation of H_2MnO requires spin crossing and is energetically unfavored due to the stability of the half-filled Mn $3d^5$ configuration.

Conclusions

The reactions of Mn atoms with water and MnO with H_2 have been studied using matrix-isolation FTIR and DFT theoretical calculations. The $MnOH_2$, HMnOH and $(H_2)MnO$ intermediates in the Mn + $H_2O \leftrightarrow$ MnO + H_2 reaction path have been observed and identified, and the potential energy surface was given. In addition, HMnOMnH, $Mn(OH)_2$, HMnOMnOH, and posssibly HMnOMnOMnH molecules were also produced on photolysis in the Mn + H_2O reaction. The aforementioned species were identified via isotopic substitutions as well as density functional theoretical frequency calculations. Scheme 1 summarizes the observed chemistry:

The spectroscopic studies of these molecules in conjunction with DFT calculations underscore the palpable differences between the Mn chemistry and the analogous chemistry with early transition metals. This work also provides a good example in demonstrating the significance of the combination of experimental and theoretical approaches in interpreting the reaction intermediates of one, two, or three metal atoms with one or two water molecules.

Acknowledgment. We acknowledge support for this research from NSFC (Grant 20003003) and the Chinese NKBRSF, and Mr. J. Dong and H.Lu for assistance with experiments.

Supporting Information Available: Detailed structural parameters, absolute energies, vibrational frequencies for different spin state molecules, and atomic spin density on Mn centers for the ground-state molecules. This material is available free of charge via the Internet at http://pubs.acs.org.

References and Notes

(1) Liu, K.; Parson, J. M. *J. Chem. Phys*. **1978**, *68*, 1794.
(2) Kauffman, J. W.; Hauge, R. H.; Margrave, J. L. *J. Phys. Chem.* **1985**, *89*, 3541.
(3) Kauffman, J. W.; Hauge, R. H.; Margrave, J. L. *J. Phys. Chem.* **1985**, *89*, 3547.
(4) Tilson, J. L.; Harrison, J. F. *J. Phys. Chem*. **1991**, *95*, 5097.
(5) Guo, B. C.; Kerns, K. P.; Castleman, A. W. *J. Phys. Chem*. **1992**, *96*, 4879.
(6) Clemmer, D. E.; Aristov, N.; Armentrout, P. B. *J. Phys. Chem*. **1994**, *98*, 6522.
(7) Chen, Y. M.; Clemmer, D. E.; Armentrout, P. B. *J. Phys. Chem*. **1994**, *98*, 11490.
(8) Ye, S. *Theochem*. **1997**, *417*, 157.
(9) Irigoras, A.; Fowler, J. E.; Ugalde, J. M. *J. Phys. Chem. A* **1998**, *102*, 293.
(10) Irigoras, A.; Fowler, J. E.; Ugalde, J. M. *J. Am. Chem. Soc*. **1999**, *121*, 574.
(11) Irigoras, A.; Fowler, J. E.; Ugalde, J. M. *J. Am. Chem. Soc*. **1999**, *121*, 8549.
(12) Irigoras, A.; Fowler, J. E.; Ugalde, J. M. *J. Am. Chem. Soc*. **2000**, *122*, 114.
(13) Rosi, M.; Bauschlicher, C. W., Jr. *J. Chem. Phys*. **1989**, *90*, 7264.
(14) Rosi, M.; Bauschlicher, C. W., Jr. *J. Chem. Phys*. **1990**, *92*, 1876.
(15) For example, see: Barber, J.; Andersson, B. *Nature* **1994**, *370*, 31.
(16) See for example: Blomberg, M. R. A.; Siegbahn, P. E. M.; Styring, S.; Babcock, G. T.; Akermark, B.; Korall, P. *J. Am. Chem. Soc*. **1997**, *119*, 8285. Aromi, G.; Wemple, M. W.; Aubin, S. J.; Folting, K.; Hendrickson, D. N.; Christou, G. *J. Am. Chem. Soc*. **1998**, *120*, 5850. Yachandra, V. K.; Sauer, K.; Klein, M. P. *Chem. Rev*. **1996**, *96*, 2927.
(17) Schröder, D.; Schwarz, H. *Angew. Chem., Int. Ed. Engl*. **1995**, *34*, 1973.
(18) Schröder, D.; Schwarz, H. *Andew. Chem., Int. Ed. Engl*. **1991**, *29*, 1433.
(19) Elkind, J. L.; Armentrout, P. B. *J. Phys. Chem*. **1987**, *91*, 2037. Georgiadis, R.; Armentrout, P. B. *Int. J. Mass Spectrom. Ion Processes* **1989**, *82*, 123.
(20) Tonkyn, R.; Weisshaar, J. C. *J. Phys. Chem*. **1986**, *90*, 2305.
(21) Stevens, A. E.; Beauchamp, J. L. *J. Am. Chem. Soc*. **1979**, *101*, 6449.
(22) Ryan, M. F.; Fiedler, A.; Schroder, D.; Schwarz, H. *J. Am. Chem. Soc*. **1995**, *117*, 2033.
(23) Chen, Y. M.; Clemmer, D. E.; Armentrout, P. B. *J. Am. Chem. Soc*. **1994**, *116*, 7815.
(24) Ryan, M. F.; Fiedler, A.; Schroder, D.; Schwarz, H. *Organometallics* **1994**, *13*, 4072.
(25) Zhang, L. N.; Dong, J.; Zhou, M. F. *J. Phys. Chem. A* **2000**, *104*, 8882.
(26) Zhou, M. F.; Zhang, L. N., Dong, J.; Qin, Q. Z. *J. Am. Chem. Soc*. **2000**, *122*, 10680.
(27) Zhou, M. F.; Dong, J.; Zhang, L. N.; Qin, Q. Z. *J. Am. Chem. Soc*. **2001**, *123*, 135.
(28) Chen, M. H.; Wang, X. F.; Zhang, L. N.; Yu, M.; Qin, Q. Z. *Chem. Phys*. **1999**, *242*, 81.
(29) Frisch, M. J.; Trucks, G. W.; Schlegel, H. B.; Scuseria, G. E.; Robb, M. A.; Cheeseman, J. R.; Zakrzewski, V. G.; Montgomery, J. A., Jr.; Stratmann, R. E.; Burant, J. C.; Dapprich, S.; Millam, J. M.; Daniels, A. D.; Kudin, K. N.; Strain, M. C.; Farkas, O.; Tomasi, J.; Barone, V.; Cossi, M.; Cammi, R.; Mennucci, B.; Pomelli, C.; Adamo, C.; Clifford, S.; Ochterski, J.; Petersson, G. A.; Ayala, P. Y.; Cui, Q.; Morokuma, K.; Malick, D. K.; Rabuck, A. D.; Raghavachari, K.; Foresman, J. B.; Cioslowski, J.; Ortiz, J. V.; Baboul, A. G.; Stefanov, B. B.; Liu, G.; Liashenko, A.; Piskorz, P.; Komaromi, I.; Gomperts, R.; Martin, R. L.; Fox, D. J.; Keith, T.; Al-Laham, M. A.; Peng, C. Y.; Nanayakkara, A.; Gonzalez, C.; Challacombe, M.; Gill, P. M. W.; Johnson, B.; Chen, W.; Wong, M. W.; Andres, J. L.; Gonzalez, C.; Head-Gordon, M.; Replogle, E. S.; Pople, J. A. *Gaussian 98*, Revision A.7; Gaussian, Inc.: Pittsburgh, PA, 1998.
(30) Becke, A. D. *J. Chem. Phys*. **1993**, *98*, 5648.
(31) Lee, C.; Yang, E.; Parr, R. G. *Phys. Rev. B* **1988**, *37*, 785.
(32) Bauschlicher, C. W. Jr.; Ricca, A.; Partridge, H.; Langhoff, S. R. In *Recent Advances in Density Functional Theory*; Chong, D. P., Ed.; World Scientific Publishing: Singapore, 1997, Part II.
(33) Bytheway, I.; Wong, M. W. *Chem. Phys. Lett*. **1998**, *282*, 219.
(34) Siegbahn, P. E. M. *Adv. Chem. Phys*. **1996**, *93*.
(35) Bauschlicher, C. W., Jr.; Maitre, P. *J. Chem. Phys*. **1995**, *99*, 3444.
(36) Hartmann, M.; Clark, T.; Van Eldik, R. *J. Am. Chem. Soc*. **1997**, *119*, 7843.
(37) McLean, A. D.; Chandler, G. S. *J. Chem. Phys*. **1980**, *72*, 5639. Krishnan, R.; Binkley, J. S.; Seeger, R.; Pople, J. A. *J. Chem. Phys*. **1980**, *72*, 650.
(38) Wachter, J. H. *J. Chem. Phys*. **1970**, *52*, 1033. Hay, P. J. *J. Chem. Phys*. **1977**, *66*, 4377.
(39) Head-Gordon, M.; Pople, J. A.; Frisch, M. *Chem. Phys. Lett*. **1988**, *153*, 503.
(40) Chertihin, G. V.; Andrews, L. *J. Phys. Chem. A* **1997**, *01*, 8547 and references therein.
(41) Ferrante, R. F.; Wilkerson, J. L.; Graham, W. R. M.; Weltner, W., Jr. *J. Chem. Phys*. **1977**, *67*, 5904. Bauschlicher, C. W., Jr.; Maitre, P. *Theor. Chim. Acta* **1995**, *90*, 189.
(42) Moore, C. E. *Atomic Energy Levels*; National Bureau of Standards: Washington, DC, 1959.]